The Mariner Spacecraft Star Sensors

W. C. Goss

The development history of the star sensors used on the Mariner spacecraft is traced, and design and performance details are described. The electrooptically controlled sensor, which was developed for the 1964 Mariner IV Mars mission, was modified for the 1967 Mariner V Venus mission to withstand the intense planetary illumination. The sensor has been further modified for the 1969 Mariner mission to Mars to survive the more severe launch environment and to provide greater capability for automatic search, identification, and tracking. Special star simulation and stray-light test techniques are discussed.

Introduction

The Mariner series of interplanetary spacecraft have all been attitude-controlled in three axes to provide a known and stable orientation during flight. Inertial sensors are used to provide short term position stability and rotation rate control. Attitude control throughout the major portion of the flight is maintained by optical sensors. An accurately controlled spacecraft orientation is needed in particular for the midcourse maneuver and during planetary encounter.

A midcourse maneuver is made—typically a week after launch—to optimize the spacecraft velocity vector. The maneuver is made under gyro control by performing two commanded turns in sequence from the base orientation to orient the thrust vector of a small rocket motor.

Planetary encounter requires the accurate pointing of the instrumentation package. Data collected must be transmitted to earth by means of the high-gain, narrow beam radio antenna.

The Mariner spacecraft have all used the sun as a yaw and pitch reference object as well as a source of electrical power. Solar panels deploy after launch to present a large surface area to the sun's illumination. Yaw and pitch attitude control is necessary to maintain a steady illumination level on the solar cells.

Mariner II, the first United States spacecraft to Venus in 1962, was roll-stabilized using the earth as a reference, as were the earlier JPL Ranger spacecraft which impacted the moon. This technique is not of general usefulness for interplanetary probes traveling in the ecliptic plane, since the sun–spacecraft–earth angle will at times pass through 0 deg or 180 deg for inner or outer planets, respectively. Also, for outer planet missions, the earth is seen in the near vicinity of the sun, and scattered sunlight makes detection difficult.

Ideally, a roll reference object for a sun-acquired spacecraft traveling in the ecliptic plane would be located at an ecliptic pole,[1] normal to the roll axis, thereby enabling the roll sensor field of view to be restricted to an angle of about 90 deg.

The best located bright star is α-Carinae (Canopus). It is the second brightest star in the sky and is situated about 15 deg from the south ecliptic pole. It has been used as a roll reference by the Surveyor and Lunar Orbiter spacecraft, as well as by Mariner IV to Mars in 1964, Mariner V to Venus in 1967, and Mariners VI and VII to Mars in 1969. Figure 1 illustrates the geometry for a sun–Canopus stabilized Mars probe.

Mariner spacecraft attitude control is typically initiated immediately after separation from the last stage rocket. Gyros provide limiting rate control and damping during the acquisition phase. Yaw and pitch acquisition of the sun is accomplished first, the spacecraft orientation being controlled so as to null the sun sensor error signals. Subsequently, the spacecraft is rolled about the sun line at a fixed rate under gyro control until Canopus enters the star sensor field of view and is acquired. Shortly thereafter, the gyros are turned off.

Control about the null point is maintained with a *deadband*. When error signal values reach the limits of the deadband, compressed nitrogen gas control jets are fired to drive the craft back toward (or through) null. This technique, rather than a proportional control, is used for simplicity and to decrease the cycling rate of the gas valves.

Basic Considerations

The Mariner star sensor performs two primary functions. It makes an identification decision on each star that enters the field of view during roll search and provides a signal proportional to the roll error angle to the attitude control circuitry when a star is identified as

The author is with the Jet Propulsion Laboratory, Pasadena, California 91103.

Received 14 August 1969.

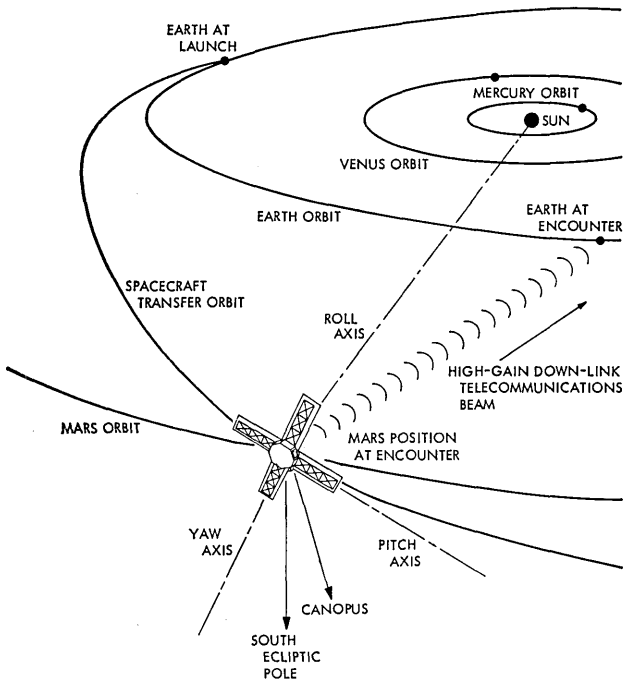

Fig. 1. Sun–Canopus-stabilized Mars probe.

Canopus. The identification process in the sensor consists of measuring the star intensity and comparing it with a previously calibrated value.

Canopus is a Type FO star with a visual magnitude of −0.86 (Revised Harvard Photometry). Norton[2] has accurately determined the absolute spectral energy distribution of illumination. An equivalent photometric illumination level is 5.49×10^{-10} cd/cm^2.

As observed with an S-11 photocathode response, Canopus has an illumination intensity about one-half that of the only brighter star, Sirius.[3] Similarly, the two next dimmer stars, Vega and Rigel, are about one-half the intensity of Canopus. This illumination intensity separation is the basis for identifying the star in flight.

Error angle information is obtained by repetitively scanning a slit field of view across the image field and then measuring the modulation phase of any star signal that appears.

Gimballing is provided to accommodate the apparent motion of Canopus. During the course of an orbit by the sun-pointing spacecraft, the star field will appear to rotate about the ecliptic pole and the sun–spacecraft–Canopus angle will vary sinusoidally, with a peak-to-peak excursion of 30 deg.

Development of the Mariner Electrostatic Image Dissector

Prior to Mariner IV, star sensor design had relied principally on mechanical devices for star signal modulation and gimballing. However, an interplanetary mission is necessarily many thousands of hours in duration, and the probability of failure of a mechanical device was considered to be unacceptably large.

A development contract was awarded to CBS Laboratories, Stamford, Connecticut, in 1961 to develop an all electrostatic image dissector[4] which would combine in one envelope the gimballing, scanning, and photomultiplier detector functions. Figure 2 illustrates the design which evolved. It was successfully flown on Mariner IV to Mars in 1964 and again on Mariner V to Venus in 1967. An improved version is on board the 1969 Mariners VI and VII to Mars.

The star field is imaged by a short focal length objective onto the S-11 photocathode. Emitted photoelectrons are accelerated by the focus electrode, and a star field image is formed by the electrons on the grounded electron aperture plate.

Those electrons which pass through the slit aperture enter a twelve-stage electron multiplier. Star field scanning and gimballing are accomplished by deflecting the electron trajectories with transverse electric fields. The Schlesinger deflectron structure has two interleaved sets of deflection plates formed to the inner surface of a cone. The deflectron has good deflection linearity and a common center of deflection for both axes.

The electrostatic image dissector has several other advantages. Imaging the photocathode upon an aperture plate limits the effective photocathode area which can contribute thermionic emission to the tube dark current. Use of electrostatic, rather than magnetic, imaging and deflection reduces power and weight requirements. In addition, interplanetary spacecraft often carry instruments sensitive to magnetic fields. Very extensive shielding would be necessary to attenuate the large volume of relatively intense fields required for magnetic deflection and focusing. Magnetic focus can provide substantially higher and more uniform image resolution than electrostatic; however, high image resolution is not a requirement for this type of star sensor. Since the sensor locates the center of illumination, the most significant requirement is long term stability of the electron image point spread function.

Figure 3 presents typical deflection characteristics of the electrostatic image dissector. The plotted points represent displacement of a point image on the photocathode from center and the corresponding deflection voltage required to displace the conjugate electron image to the aperture plate center.

Figure 4 illustrates the electron image diameter

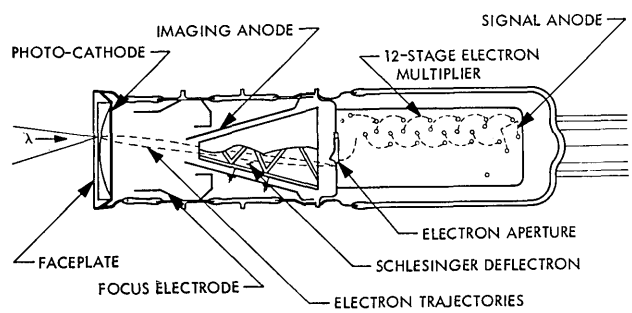

Fig. 2. The Mariner electrostatic image dissector.

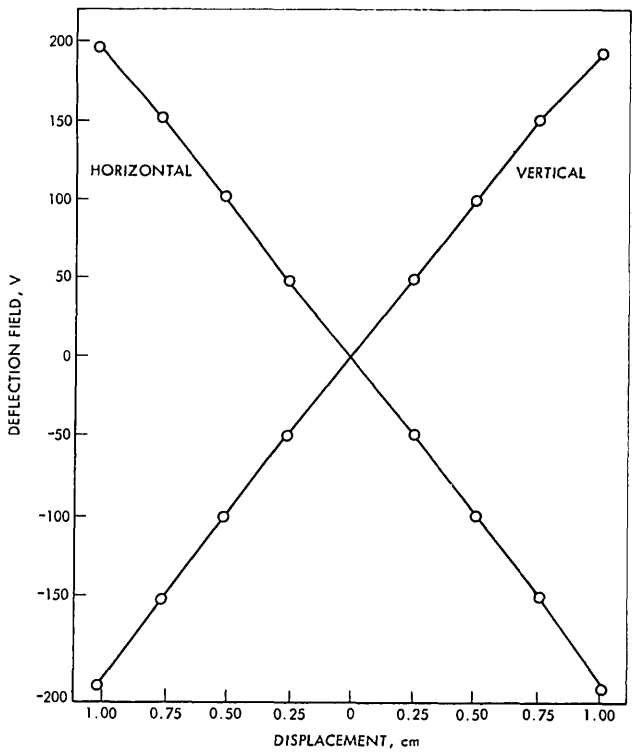

Fig. 3. Mariner image dissector deflection characteristics.

variation with displacement of the optical image from the photocathode center.

Mariner IV Star Sensor[5]

Star Identification

Identification of Canopus was not an automatic function for the Mariner IV sensor. Low- and high-intensity gates, set at $\frac{1}{4}$ and 8 times the value for Canopus, were used to limit the number of celestial objects that could be acquired. Positive identification of the star was based on a star map matching technique.

After sun acquisition, the spacecraft rotated about the sunline, searching for a star that would meet the requirements of the gates. As each successive star passed through the sensor field of view, the measured illumination value was telemetered to earth, decoded, and printed on a strip chart at the Jet Propulsion Laboratory (JPL). A predicted star map overlay, made to the same scale as the strip chart presentation, was used manually to obtain an identification by correlation in real time. Acquisition of a wrong star was corrected by a radio command to disacquire and continue roll search.

The predicted star maps were generated by a 7094 computer program which stored the coordinates and effective intensity ratios of 423 stars in addition to brightness contours for the Milky Way and the Zodiacal Light. The program, known as SIPM (Star Identification Program, Mariner), mathematically modeled the star sensor field of view coverage and response characteristics to generate predicted star maps for any given roll axis orientation.

Functional Characteristics

The Mariner IV star sensor weighs 2.27 kg and consumes 1.5 W of electrical power. Exterior dimensions are 11.1 cm wide × 13.3 cm high × 28.6 cm long.

Table I lists the characteristics of the roll error angle transfer function for both the Mariner 1964 and Mariner 1969 star sensors. A typical Mariner IV roll error transfer function is shown in Fig. 5. Note that the illustrated range of fifteen to one in star illumination did not measurably shift the roll error function null point.

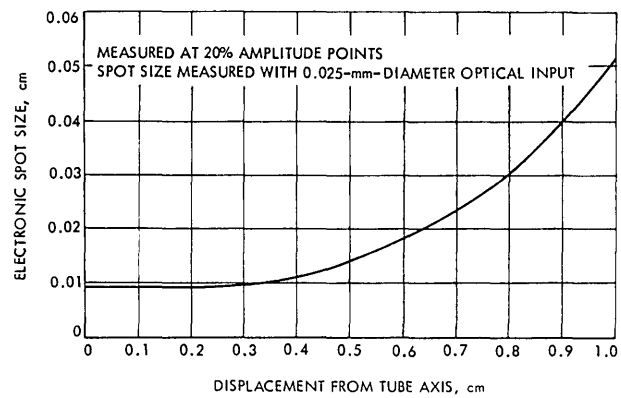

Fig. 4. Mariner image dissector electronic spot size.

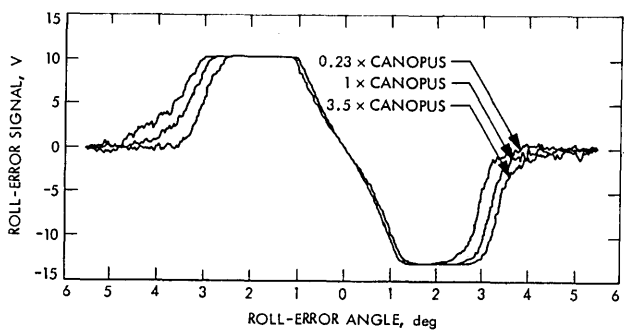

Fig. 5. Mariner IV star sensor roll error transfer function.

Table I. Characteristics of the Mariner Star Sensor Roll-Error Transfer Functions

Characteristic	Mariner 1964, 1967	Mariner 1969
Linear range, deg	±0.85 ±0.15	±3.25 +1.0 −0.75
Saturated range, deg	±2.0, minimum	±5.0 +1.6 −0.9
Scale factor, V/deg	8 ± 1.6	3.7 ± 0.6
Angle noise, deg rms	0.005, typical	0.005, typical
Time constant, sec	0.5, maximum	0.5, maximum
Null accuracy, deg	±0.125, maximum	±0.05, maximum

Figure 6 illustrates a typical star intensity signal as a function of star roll error position. Note the inverse logarithmic response to illumination level.

Typical high and low gate level limits are shown. The "low gate" and "low gate hysteresis" limits refer to those levels at which a star will be acquired as it comes into the field of view and disacquired if it should leave the field of view. An acquisition signal is sent to the attitude control logic when a star intensity signal is measured as being within the gate limits.

The variation of sun–probe–Canopus angle (Canopus cone angle) during the time from launch to encounter was so wide as to make coverage by a single field of view undesirable. The Mariner IV star sensor nominally covers 11 deg in cone angle with provision to step the field of view in a sequence of six overlapping positions to cover the required 34 deg. The spacecraft was launched with the sensor preset to the first position; thereafter, steps were made in response to commands issued from the central computer and sequencer (CC&S) on board the spacecraft. A radio command capability existed to back up the on-board command.

Since the image dissector photocathode would be severely damaged if sunlight were to be focused on it, a rotary solenoid sun shutter is mounted in front of the sensor. A sun detector, built into the sensor housing and aligned with the optical axis, provides a means of sensing the near approach of sunlight and triggers closure of the shutter. Figure 7 illustrates the limiting threshold illumination values, as a function of angle from boresight, at which the shutter will be closed. Both the roll angle and cone angle offset functions are presented in Fig. 7, as the functions are symmetrical about the optical axis.

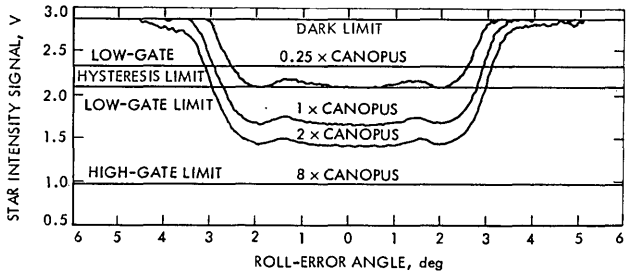

Fig. 6. Mariner IV star sensor intensity signal variation with roll error angle.

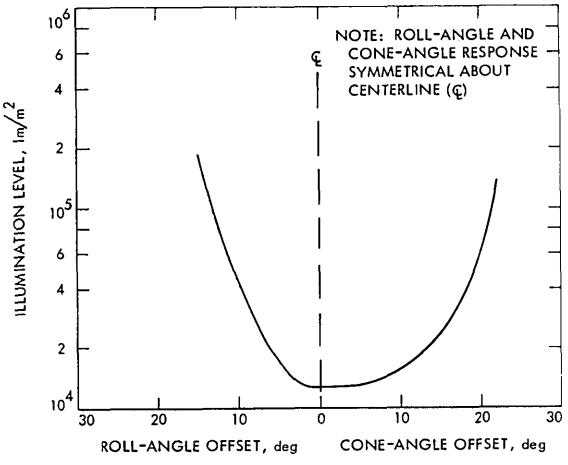

Fig. 7. Mariner IV sun detector trigger level as a function of illumination and angle from boresight.

Mechanization

Figure 8 is a functional block diagram of the Mariner IV star sensor. The star field is imaged onto the image dissector photocathode by an $f/1.0$ objective lens of 2.0-cm focal length. The conjugate electron image is sinusoidally scanned 4 deg peak-to-peak across the 0.85 deg wide slit aperture. The resulting signal is processed by a half-wave phase-sensitive demodulator to develop the error angle signal and by a peak detecting circuit to measure the star illumination intensity.

The peak detector output is compared against a reference level. The difference signal is fed into an automatic gain control (AGC) loop which varies the electron multiplier voltage. The AGC circuit limits the amount of current that may be drawn from the tube and, by maintaining a constant amplitude star signal over a wide range of star intensity, simplifies the design requirements of the signal processing circuitry. The intensity signal, which is telemetered to earth, is divided down from the multiplier high voltage and so is related in an inverse logarithmic way to the star illumination level.

Figure 9 illustrates the waveforms generated by a star image whose mean position is (a) centered on the electron aperture, (b) displaced by a half scan width,

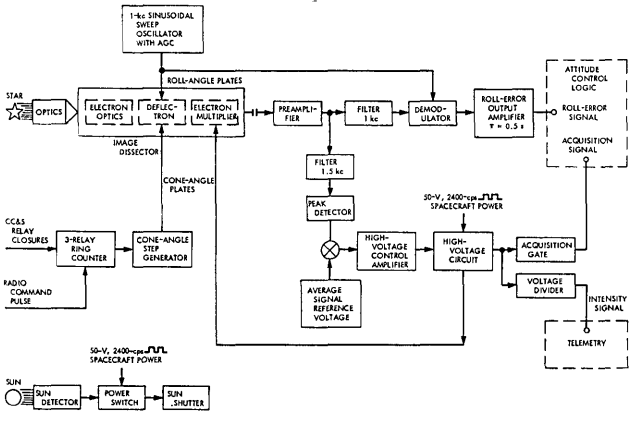

Fig. 8. Mariner IV star sensor functional block diagram.

and (c) displaced by a half scan width in the opposite sense. Note the absence of a 1-kHz component in case (a) and the half-cycle phase shift in the 1-kHz component between cases (b) and (c). Thus, the 1-kHz component changes sign and goes through zero as the error angle

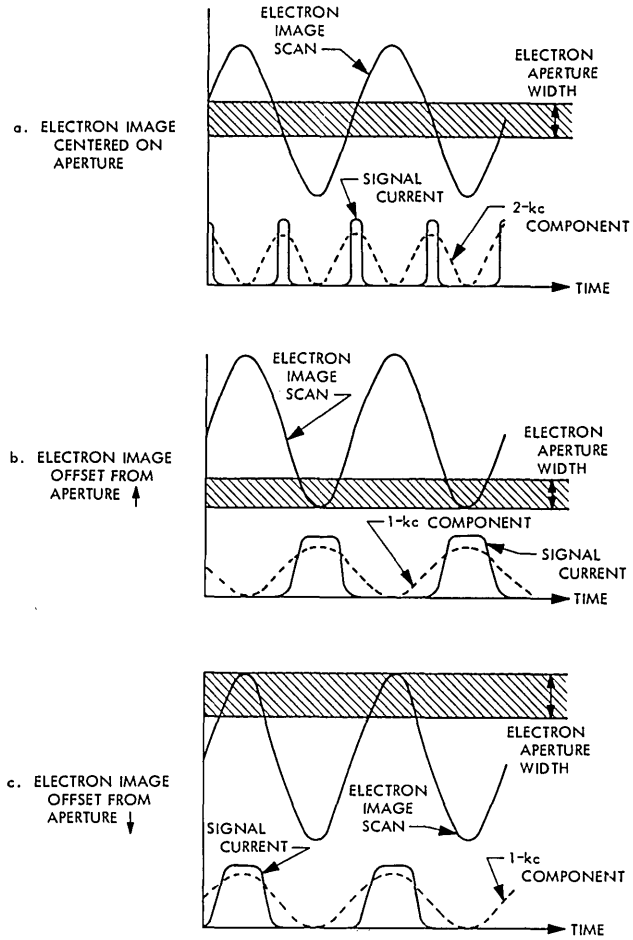

Fig. 9. Mariner IV star image scan and signal waveform.

goes through null. This component is isolated, conditioned, and then delivered to the attitude control logic as the roll error angle signal.

The design requirements on the optical components were to provide uniform sagittal resolution and image illuminance over a full field of view of 4 deg × 30 deg, measured at the image dissector photocathode. This is a backward-curving surface as seen from the objective lens. The design solution was to use a catadioptric objective to form a flat field image onto the front surface of the image dissector faceplate. The faceplate was fabricated of sealed fiber optics and the photocathode formed directly on the inner surface.

The sun detector consisted of a cadmium sulfide photoresistive cell mounted behind a rectangular aperture to provide the field of view limits. The sun shutter was a blade attached to a commercial rotary solenoid modified for vacuum operation.

Calibration and Test

Calibration of the Mariner IV Mars star sensor to determine the response to Canopus was performed using several independent techniques to obtain an over-all best estimate. Field tests were performed at Santiago, Chile, to determine the star sensor response ratio between Sirius, which can be usefully observed in the USA, to Canopus, which cannot. Subsequent sensor calibrations were made by observing Sirius at a field station in the San Gabriel Mountains to the north of Pasadena.

In addition to the field measurement technique, which had the disadvantages of transfer calibration, air mass uncertainties, weather dependence, and logistics, two laboratory simulation standards were constructed and the resulting sensor calibrations compared. The simulations were based upon a knowledge of the absolute spectral energy density of the sources, the absolute spectral energy density of Canopus as reported by Norton,[2] and the spectral response characteristics of each individual star sensor. One simulator was built with a high-pressure xenon arc and calibrated with a spectroradiometer by comparing at discrete wavelengths with a National Bureau of Standards (NBS) ribbon filament standard lamp. The second simulator was built with the new quartz envelope tungsten–iodine NBS standard lamp. The worst case calibration error of the flight unit star sensor is estimated to have been ±26% and the probable error ±11%.

In addition to a full set of functional, illumination background, and stray light tests, the sensor was successfully subjected to a wide variety of conditions and environments intended to determine operability under the worst circumstances likely to be encountered. It was subjected to power supply voltage and frequency variations, thermal vacuum tests, vibration and shock, humidity, static acceleration, and electron and proton bombardment.

In-Flight Performance[6]

The initial roll search for Canopus on 29 November 1964, resulted in a number of acquisitions: a stray light pattern from the near earth, Alderamin, Regulus, Naos, γ Velorum, and finally, Canopus. There was an unmistakable correlation between the features of the predicted and telemetered maps, and the predicted and measured values for Canopus agreed within the telemetry bit width of about 13%.

A consistent problem that plagued the spacecraft during the early portion of the mission was that roll error signal transients occurred frequently, occasionally causing loss of Canopus lock. The first attempt at a midcourse maneuver was aborted by a loss of lock shortly after the gyros began spinup. Canopus lock was lost six times within a period of less than 3 weeks after launch, each time necessitating a sequence of radio commands to reacquire the star.

Analysis and tests of possible mechanisms that could cause this behavior led to the conclusion that small dust particles were being released from the spacecraft by some means and were drifting through the star sensor field of view. Sunlight scattered from the particles then appeared as illumination equivalent to that from a bright star. Understandably, a roll error transient would occur if a bright object passed through the field

of view while the sensor was locked on Canopus. If the object appeared bright enough to exceed the high gate limit at eight times Canopus intensity, the spacecraft would automatically disacquire Canopus and initiate roll search for a new star.

A radio command was sent on 17 December 1964, which effectively removed the high gate limit. There was no further loss of Canopus lock, although roll transients occurred thirty-eight more times before planetary encounter.

The dust particle theory appears to be very plausible. A 25-μ translucent dust particle with a diffuse scattering coefficient of 0.4 would appear as bright as Canopus at a distance of 66 cm. Large numbers of dust particles of this size and larger are collected on exposed surfaces even in the controlled environment of a spacecraft assembly area. The forces which cause dust particles to adhere to a surface are very weak, and a minor vibration or shock event may release them. It may possibly be significant that of the four events on the spacecraft which represented a mechanical disturbance, two were attended with roll transient events. One was the initial attempt at a midcourse maneuver, entailing gyro runup, and the other was a science instrumentation cover deployment. Micrometeorite impacts have been proposed as a continuing release mechanism.

Aside from the roll transient events, the Mariner IV star sensor performed as designed throughout the mission and beyond, to the end of the life of the spacecraft. Exercises with the spacecraft were continued after Mars encounter to ascertain equipment condition as facilities, personnel, and communications distance allowed, until 15 December 1967. Literally "out of gas" on that date, the spacecraft was determined to be in a fast nutating roll about the sunline. Communications were reduced to those few moments each period when the high gain antenna was pointed toward earth. Tracking was terminated on that date.

Mariner V Star Sensor[7]

Ground Rules for Changes

The Mariner V Venus spacecraft was a minimum change version of the successful Mariner IV. The design was considered frozen at the outset, and only changes that could be proved necessary were allowed. Flight-qualified spare hardware from the Mariner IV Project was upgraded, tested, requalified, and redelivered to the Mariner V Project.

Allowed changes were principally those made because of differences in planetary conditions, problems encountered on the Mariner IV mission, or the current nonavailability or obsolescence of components previously used.

Star Sensor Logic Changes

Turning the spacecraft around to point the instrument package toward an inner planet necessitated relocating the star sensor on the opposite (dark) end of the spacecraft. This required a change in polarity of the transfer function, which was accomplished quite simply by exchanging the sweep signal leads to the image dissector deflectron.

To minimize the effects of a repetition on Mariner V of the Mariner IV experience with roll transients, the high gate limit was effectively removed by setting it to infinity. The intent of the Mariner IV high gate was to prevent acquisition of the earth and possible damage to the image dissector photocathode due to long exposure. None of the standard Mariner V trajectories brought the illuminated portion of the earth directly into the sensor field of view.

In addition, the low gate limit was increased to 0.5 of the Canopus level, reflecting a considerable increase in confidence in the calibration.

Stray Light Sensitivity Reduction

The major effort in upgrading the star sensor was devoted to obtaining adequate stray light rejection at planetary encounter to ensure continued roll control. The relative solar constants and apparent surface albedos combine to make the Venus atmosphere appear about fifteen times as bright as the surface of Mars.[8] Worst case estimates of Venus illumination on the sensor were in excess of 10^4 lm/m^2, a factor of 2×10^9 times the illumination from Canopus.

Since the planet would subtend angles greater than 90 deg, the planetary surface brightness distribution was a necessary factor in predicting sensor performance.

The model adopted for the diffuse reflectivity of the Venusian atmosphere assumed the reflectivity to be due to a single scattering process, with the scattering coefficient a function of the scattering angle only. The planetary phase illumination function as seen by a distant observer then is related simply to the scattering function. The model was programmed for the IBM 7094 computer using values tabulated by de Vauc-

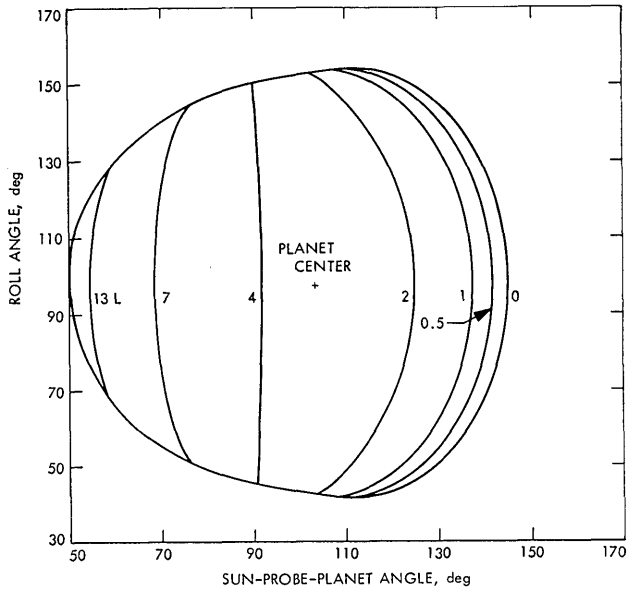

Fig. 10. Predicted surface brightness contour of Venus at Mariner V encounter, worst case.

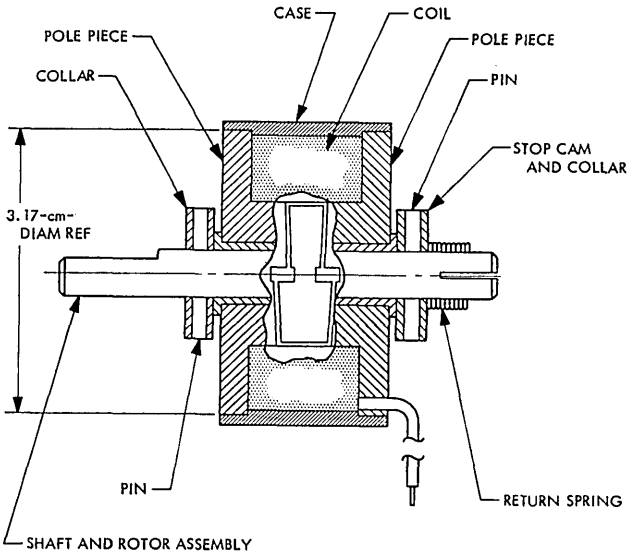

Fig. 11. Mariner V star sensor sun shutter rotary solenoid.

ouleurs.[8] Figure 10 illustrates the surface brightness prediction made by this program for the least favorable encounter geometry. The coordinates are referenced to the spacecraft, assuming the craft is Canopus-oriented at star sensor null.

Star sensor stray light response data taken during the Mariner IV flight indicated that the worst case trajectory Venus illumination would exceed the safe limits by more than an order of magnitude. Two steps were taken to improve the stray light rejection. A baffle box that could be mounted to the front of the sensor was built, and concurrently, since wide angle baffle dimensions are a sensitive function of the entrance pupil diameter, the objective lens was redesigned. An all refractive objective was designed with a JPL adaptation of the Los Alamos automatic lens design code,[9] reducing the entrance pupil diameter from 3.37 cm to 1.47 cm.

Sun Shutter Solenoid Redesign

The presence of the baffle box eliminated the possibility of using the Mariner IV externally mounted shutter. A new design was developed and mounted internally. The new unit is a true rotary solenoid, developing rotation without axial travel by means of a helically cut rotor mounted between helically faced pole pieces (Fig. 11). This approach eliminates the problems of lubricating balls and inclined races for vacuum operation. To date, one unit has been tested in a simulated space environment for $\frac{1}{2}$ million cycles, another in a laboratory life test for 36 million cycles.

Vacuum Stray Light Tests

The predicted worse case illumination values (13,560 lm/m^2) from Venus were too great to be tested in the usual darkroom facility. The Mariner V star sensor was very sensitive to low level brightness backgrounds because of the wide bandpass of the intensity peak detecting circuit, a background brightness of 1×10^{-6} lamberts (L) appearing nearly as bright to the sensor as Canopus. Even Rayleigh scattering from the air within the minimum cross section beam necessary to conduct the test exceeded the allowable background brightness.[7]

A stray light test fixture that could be used in a 2-m diam $\times$ $4\frac{1}{4}$ m long vacuum chamber is shown schematically in Fig. 12. A 1000-W quartz envelope tungsten–iodine lamp in a PAR bulb configuration provided the stray light source. The lamp was mounted on a sealed flex hose-coupled housing and was cooled by a flow of air. The lamp could be driven along a track to change the distance to the test fixture; in addition, the angle of incidence of the beam on the sensor test mount could be varied from 36 deg to 90 deg. The maximum attainable illumination level on the test article was 200,000 lm/m^2.

The sensor was mounted face down from a motor-driven mount that allowed essentially full rotation about the optical axis. The sensor viewed a light trap disk of black anodized aluminum honeycomb, bonded to a black anodized aluminum baseplate, as seen reflected from an inclined black glass surface. A star source collimator was mounted in the disk, and the entire disk and collimator assembly could be rotated to match the rotation of the sensor.

The honeycomb material was 7.62 cm thick and had a cell width of 9.5 mm and a cell wall thickness of 0.017 mm. Measured diffuse reflectivity was typically 2×10^{-3}. Liberal use was made of this material on all exposed surfaces to absorb stray illumination.

The background brightness seen by the sensor at 13,560 lm/m^2 was, under worst case conditions, 6.2×10^{-4} cd/m^2. Test results[8] indicated that a worse case null offset of $\frac{1}{4}$ deg in roll could occur at encounter. This was an acceptable value.

Calibration

The Mariner V star sensors were calibrated by a single simulator technique and checked against Mariner IV units which still maintained their calibration. The most accurate and reproducible calibration technique

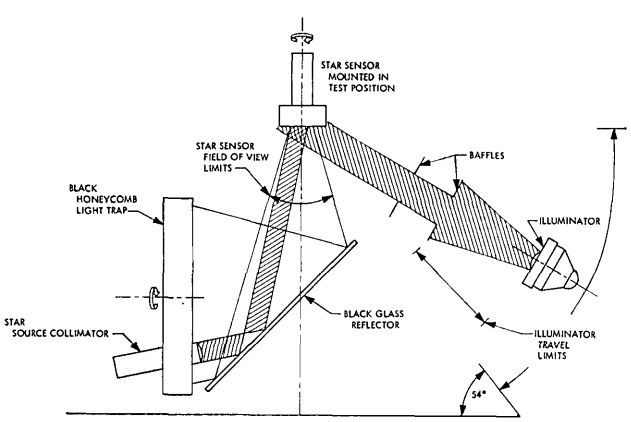

Fig. 12. Vacuum stray light test fixture.

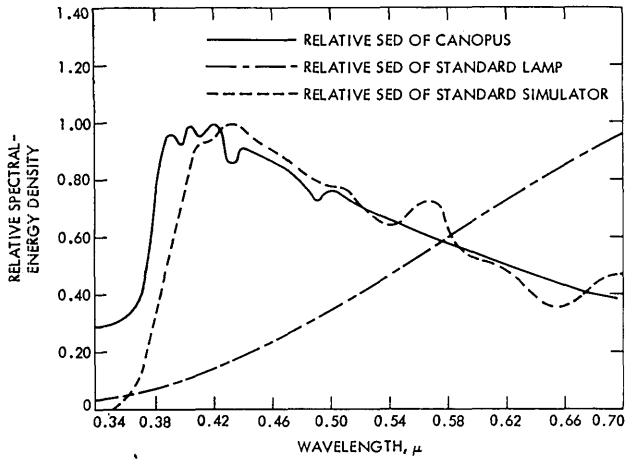

Fig. 13. Relative spectral energy density of Canopus, the NBS 1000-W standard lamp, and the JPL standard Canopus simulator.

employed during the Mariner IV Project had been the use of the National Bureau of Standards 1000-W quartz envelope tungsten–iodine lamp. Although the 1000-W standard has a spectral emission curve grossly different from the Canopus distribution, the values are known with a relatively small error and change very little during the lamp life, so that a calibration value can be precisely calculated. This technique is dependent on accurate measurements of the individual sensor spectra response characteristics.

The significant factor in the simulation equation is the integral ratio

$$I = \int^{\lambda} D(\lambda)L(\lambda)d2 \int^{\lambda} D(\lambda)C(\lambda)d2,$$

where $D(\lambda)$ is the sensor response, normalized to unity at peak; $L(\lambda)$ is the simulator spectral energy distribution, normalized to unity at peak within the integration interval; $C(\lambda)$ is the Canopus spectral energy distribution, normalized to unity at peak.

Note that if a filter with transmission function $F(\lambda)$ can be found such that $L(\lambda)F(\lambda) = kC(\lambda)$, then I is identically k and the calibration is no longer dependent on the spectral response of the sensor.

A glass filter of suitable spectral characteristics and long term stability (Corning 1-62) was found and was fabricated to the correct thickness, calibrated at NBS, and installed in a standard Canopus simulator at JPL. Figure 13 illustrates the relative spectral energy densities of Canopus as given by Norton,[2] the NBS 1000-W standard lamp, and the standard Canopus simulator. The integral ratio I is 0.92 for this simulator and an S-11 response, cut off at 0.38 μ by the objective lens. The calibration variance due to individual Mariner star sensor spectral response variations is less than 1%.

In-Flight Performance

In-flight performance was entirely nominal.[10] A stray light reflection from the near earth was first acquired, as had been predicted by the SIPM program. Radio commands were sent to override the acquisition, and the spacecraft rolled on, ignoring all other stars as being below the low gate limit, until Canopus was reached and acquired. Reacquisition after the midcourse maneuver was similarly uneventful. Star intensity telemetry data agreed with the preflight calibration data to within several percent, although telemetry quantization uncertainty necessarily added $\pm 6\frac{1}{2}\%$ to that number.

The sunlit dust phenomenon was noted again. More than twenty roll transients were observed during the flight, but none caused loss of lock. Flyby of the planet Venus occurred under star sensor roll control without anomaly.

Mariner VI and VII Star Trackers

Design Changes

A number of new requirements led to a very substantial redesign of the star sensor for the Mariner Mars 1969 program. The policy of developing a basically automatic spacecraft, for which radio commanded operation would be largely a backup mode, had the greatest impact. A larger and more effective baffle and a new intensity measuring circuit which was relatively insensitive to noise signals were designed to eliminate the problem of earth stray light acquisitions. A substantial amount of logic circuitry was included to allow use of a high gate limit without compromising the dust particle rejection technique used on Mariners IV and V, and to automatically provide successively lower gate limits in the event of image dissector degradation.

The estimates of the launch vibration were severely increased over that for Mariner V, reflecting the change in launch vehicle from an Atlas/Agena to an Atlas/Centaur. This necessitated a general strengthening of the entire assembly, and for some components, a complete redesign.

In conjunction with a faster spacecraft roll search rate, nominally increased from 1.7 mrad/sec to 3.5 mrad/sec, the linear portion of the roll error transfer function was widened to a nominal 6.5 deg. The wider field allowed for an increased spacecraft overshoot due to the increased roll search rate. This was accomplished by feeding back the phase demodulation generated roll error signal to the deflection plates so that the field of view would center on and track a recognized star. The roll error signal delivered to the attitude control circuitry was then taken from the deflection plate voltage.

The field of view cone angle position sequence was modified to provide continued coverage past encounter in anticipation of a postencounter mission.

In addition, some components were changed because of obsolescence or difficulty of fabrication, or because parts having similar characteristics and better reliability histories were available.

Figure 14 shows the 1969 Mariner star tracker, with the stray light baffle and sun detector in place. Two units are being flown on the spacecraft designated as Mariner VI and VII.

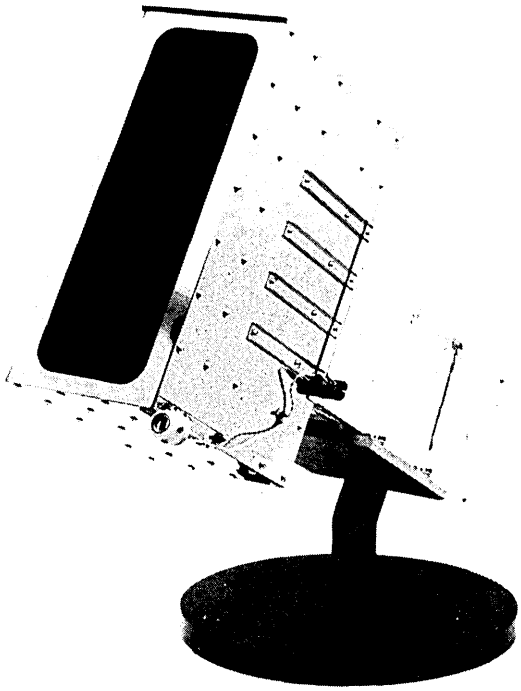

Fig. 14. Mariner Mars 1969 star tracker.

Functional Characteristics

In addition to providing a wider roll error transfer curve by closing the roll control loop in the star tracker, a further improvement was gained in the linearity of the function. The signal trace shown in Fig. 15 represents six superimposed data recordings made with star source intensities ranging from 0.03 to 2.0 that of Canopus, illustrating roll error function independence of that parameter.

Note that the roll error signal returns to −13 V dc for roll angles nominally less than −5 deg. The field of view is mechanized to return to the positive roll angle side whenever there is no star acquisition, in which case the spacecraft will normally be in a roll search, rolling so that the stars enter the field of view from that side.

Figure 16 illustrates a typical star intensity signal function for the Mariner Mars 1969 star tracker. The successive low gate levels shown are the three possible states for the low gate circuitry. If no star can be found in gate level 1, the tracker is automatically stepped to gate 2. The sequence steps are 1, 2, 3, 1, 2...

The nominal high and low gate levels are set at 3.9 and 0.7 times Canopus, excluding all stars except Sirius. Vega is close on the low end, and was, in fact, acquired by the Mariner VII star tracker, which exhibited a variable sensitivity for a short period following turn-on.

Cone angle field of view coverage was increased to 11.8 deg nominal length, and the total number of positions reduced to five. This number most easily accommodates the requirements for an ascending then descending sequence to follow the Canopus cone angle variation. A three-element binary counter provides eight states, the number required to count from 1 to 5 and back to 2.

The high gate input to the recognition logic is automatically removed after Canopus has been acquired and the spacecraft roll position has stabilized with the star at null in the tracker field of view. Thus, in the event of sunlight illuminated debris passing through the field of view and adding to the star illumination, a high gate violation will not cause the star to be disacquired. The high gate is reset only if the measured illumination subsequently falls below the low gate hysteresis level long enough for the acquisition signal to be dropped.

In the event that Canopus is lost after having once been recognized and acquired, the field of view steps immediately to the roll angle limit opposite the bias position and then executes a single sweep search for the star, ending at the bias position, if the search has been unsuccessful. The acquisition signal is then dropped, and the attitude control electronics initiate spacecraft roll search under gyro rate control.

Judging from previous flight experience, the most probable cause of an event of this type is a disturbance in which a dust particle is dislodged from the spacecraft and crosses the tracker field of view. If it is brighter than Canopus, the field of view follows it and the spacecraft accelerates in that roll direction. Because of initial velocity or solar pressure acceleration, a single dust particle usually passes through the field of view quickly, and the tracker sweep search locates Canopus once it is gone. However, if a single particle, or a succession of particles, remains in the tracker field of view long enough for the spacecraft to roll away from Canopus, the subsequent sweep search finds nothing, and gyro-controlled roll search is initiated.

In the event of a logic element failure in the tracker or a major degradation of sensitivity, a backup mode of operation can be initiated by radio command. In this

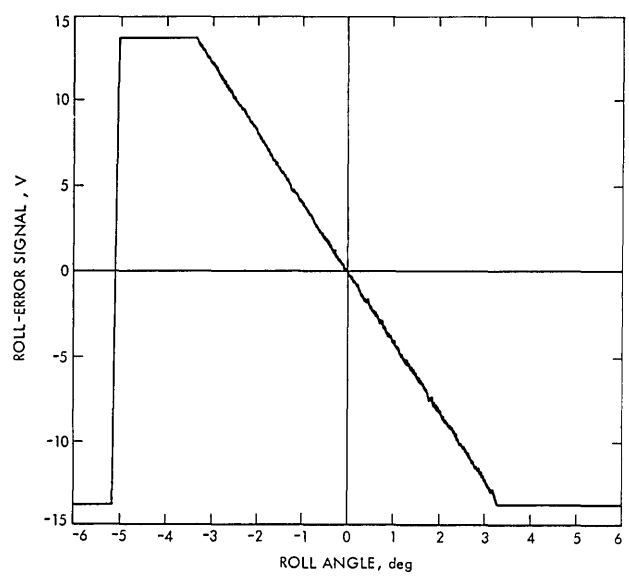

Fig. 15. Mariner Mars 1969 star tracker roll error transfer function.

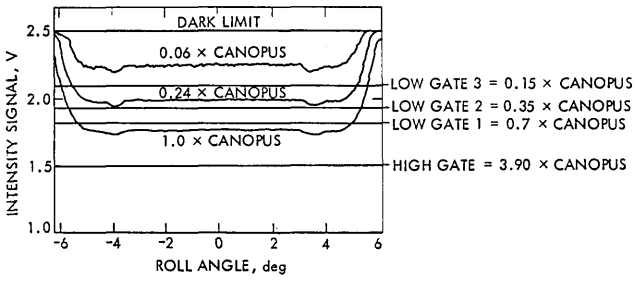

Fig. 16. Star intensity signal as a function of roll angle and star illumination level relative to Canopus.

mode, all acquisition and tracking logic elements are bypassed in the star tracker, and Canopus identification is accomplished by manual star map matching as for the earlier sensors. The field of view is held in the search position in this mode by a small bias current that is overridden when a recognizable star comes into view. With normal sensitivity, the tracker can recognize and track any object appearing brighter than about $\frac{1}{30}$ of Canopus. A commanded turn under gyro control to plot a star map would normally be made under these circumstances, with a second commanded turn terminating with the tracker oriented to Canopus.

Table II summarizes the Mariner Mars 1969 star tracker functional characteristics.

Mechanization

Figure 17 is a block diagram of the star tracker. Note that the roll error demodulator output is integrated and drives deflection amplifiers which close the roll loop with the image dissector Deflectron roll plates.

The remodulator circuit is an active filter which synchronously peak detects the in-phase and quadrature signal components. The signals are then summed and directed to the high-voltage power supply circuit to complete an AGC loop as before. This change significantly reduces the tracker intensity response to nonstar sources, such as the Milky Way or diffuse stray light illumination.

The stray light baffle is large (approximately 30 cm × 18 cm × 13 cm) compared with the one used for the Mariner V star sensor and reflects the emphasis placed on decoupling the tracker from bright objects outside the field of view. It is fabricated of 0.13-mm formed and riveted stainless steel sheet pieces and weighs about 658 g. All internal surfaces are finished flat black, with epoxy paint. The baffle plate edges are machine cut to a knife edge to reduce edge scattering.

To reduce the costs and problems of fabrication, the fiber optics faceplate of the image dissector was replaced with a clear glass faceplate for the Mariner Mars 1969 tracker design. A new objective lens was designed to provide an image which would fit the backward-curving photocathode surface and provide sagittal image width complementary to that of the image dissector electron optics. By this means, the electron image with in the scanning direction at the aperture plate is held relatively constant, and the modulation waveform changes little with field angle.

All lens elements are antireflection coated with a broadband three-layer coating. Limiting ray profiles were calculated and unused lens surface areas finished black with epoxy paint.

Table II. Mariner Mars 1969 Star Tracker Functional Characteristics

Functions	
Automatic	Commanded
Star illumination measurement	Field of view cone angle step (by CC&S and radio command)
Canopus identification and tracking	Low gate level step (by A/C and radio command)
Roll error angle measurement	Star disacquisition (by radio command)
Field of view search	
Sun shutter actuation	
Tracker temperature measurement	
Modes of operation	
Automatic	Backup—logic bypassed. No star illumination gates
Unacquired. Field of view biased to search position	Unacquired. Field of view biased to search position
Acquired tracking	Acquired tracking
Single sweep search of field of view. Occurs only after loss of lock	

Special Testing

Tests were made of the stray light response for each flight unit star tracker. Figure 18 plots the stray light illumination level vs position angle function for which

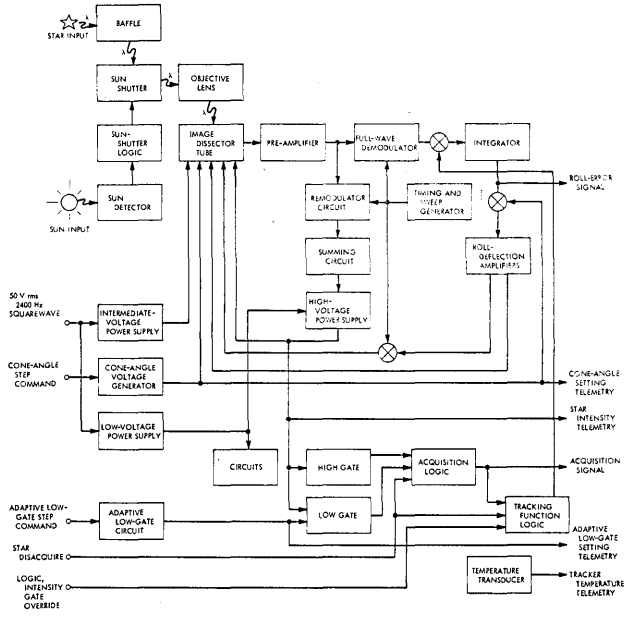

Fig. 17. Mariner Mars 1969 star tracker block diagram.

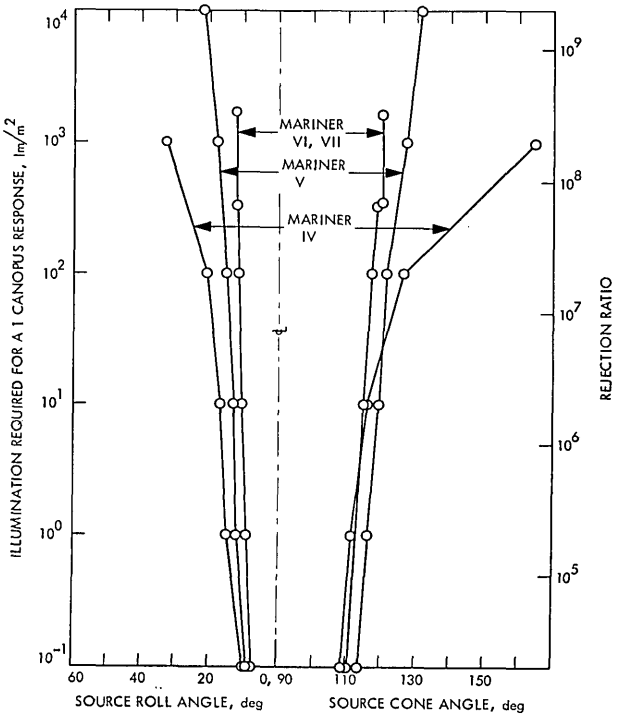

Fig. 18. Mariner sensor stray light response functions.

the tracker will give a one times Canopus intensity readout. Since the functions are basically symmetrical about the optical axis, functions for both roll and cone angle offsets are displayed on the same graph. The Mariner IV and V stray light response functions are shown for comparison.

Since the illuminated earth crescent could be expected to pass through the tracker field of view during roll search at initial acquisition for some launch dates, a series of tests was run to determine whether the earth would be acquired. The tests showed that the high stray light rejection function plus the high and low gate logic would discriminate against the earth for all cases except two. If earth illumination passed directly down the optical axis of the instrument, weak multiple reflections in the lens elements would provide a variety of star-like images, causing an unstable acquisition. The second case would arise if the illuminated earth were located at the proper cone angle offset to produce an effective response within the gate levels. This condition would have existed for the days of 1 March–3 March 1969, had Mariner VI or VII been launched during that period.

Flight Performance

Flight performance of the Mariner VI and VII trackers has been as predicted,* except for a problem diagnosed as an intermittent relay in the cone angle switching circuit of Mariner VI. Canopus intensity calibration again was close—within 5% for Mariner VI and 8% for Mariner VII.

The improved background rejection of the new tracker improved the correlation with the SIPM roll map predictions. Figure 19 illustrates the predicted and actual star map for the Mariner VI initial roll search. By chance, the Mariner VI roll search was begun in a roll position past the earth, and the earth light rejection capability was not exercised. The Mariner VII tracker did roll through the earth light region without incident.

The stray dust problem is still with us. Several roll error events have been noted in cruise to date that were attributed to single dust particles. No loss of lock due to these occurrences has been experienced. However, violent responses have been observed on the roll error channel during the midcourse motor burn and after explosive valve firings on both Mariners VI and VII. Apparently, large numbers of dust particles were released from the spacecraft. Star sensor power was not on at similar event times for the Mariner IV and V missions so this behavior had not previously been observed.

As a result, it is anticipated that similar dust disturbances might occur during planetary encounter. A scan platform will be in motion during this time aiming the television and scientific instrument package, and a cryogenic unit will be discharging a gas flow. Accordingly, the spacecraft has been programmed to transfer to gyro roll control for the flyby period, with the star tracker roll error telemetry providing a continuing measurement of spacecraft roll attitude.

This paper presents the results of one phase of research carried out at the Jet Propulsion Laboratory, California Institute of Technology, under Contract No. NAS 7-100, sponsored by the National Aeronautics and Space Administration.

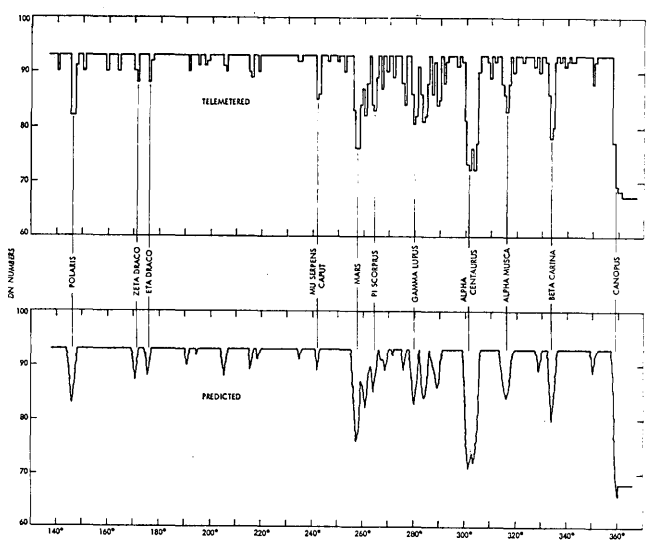

Fig. 19. Mariner VI initial roll search star map.

* As of the time of writing, July 1969.

References

1. J. R. Scull, *The Application of Optical Sensors for Lunar and Planetary Space Vehicles*, AGARDograph 71 (Pergamon Press, New York, 1961), pp. 395–410.
2. R. H. Norton, "The Absolute Spectral-Energy Distribution of Canopus," Tech. Rept. 32-641, Jet Propulsion Laboratory, Pasadena, Calif., 15 August 1964.
3. P. Haskell, "Star Tables for Satellite Attitude Control," Royal Aircraft Establishment Tech. Rept. 68048, February 1968.
4. P. T. Farnsworth, J. Franklin Inst. **218**, 411 (1934).
5. G. Meisenholder and E. Davis, paper presented at 16th International Astronautical Congress, September 1965, Athens, Greece.
6. "Mariner Mars 1964 Project Report: Spacecraft Performance and Analysis," Tech. Rept. 32-882, Jet Propulsion Laboratory, Pasadena, Calif., 15 February 1967.
7. "Mariner Venus 1967 Final Project Report: Volumes 1 and 2," Tech. Rept. 32-1203, Jet Propulsion Laboratory, Pasadena, Calif., 15 June 1968.
8. G. de Vaucouleurs, "Phase Curves and Albedos of Terrestrial Planets," AF 33(616)-7413, 11 (June 1961).
9. B. Brixner, Appl. Opt. **2**, 1281 (1963).
10. Space Programs Summary 37–45, Vol. 2, Jet Propulsion Laboratory, Pasadena, Calif., 15 June 1968, pp. 31–35.